Wind and Structures, *Vol. 31, No. 3 (2020) 185-196*
DOI: https://doi.org/10.12989/was.2020.31.3.185

Reducing the wind pressure at the leading edge of a noise barrier

Seong-Wook Han[1a], Ho-Kyung Kim*[2], Jun-Yong Park[3b] and Sang Sup Ahn[4c]

[1]Department of Infrastructure Safety Research, Korea Institute of Civil Engineering and Building Technology, 283 Goyangdae-ro, Ilsanseo-gu, Goyang-si, Gyeonggi-do 10223, Republic of Korea
[2]Department of Civil and Environmental Engineering, Seoul National University, 1 Gwanak-ro, Gwanak-gu, Seoul 08826, Republic of Korea
[3]Department of Urban Infrastructure, Seoul Institute of Technology, 37 Maebongsan-ro, Mapo-gu, Seoul 03909, Republic of Korea
[4]Structure Research Division, Korea Expressway Corporation Research Institute, 24 Dongbusunhwan-daero 17-gil, Hwaseong-si, Gyeonggi-do 18489, Republic of Korea

(*Received August 23, 2018, Revised July 9, 2020, Accepted August 11, 2020*)

Abstract. A method to reduce the wind pressure at the leading edge of a noise barrier was investigated by gradually lowering the height of a member added to the end of the noise barrier. The shape of the lowered height of the added member was defined by its length and slope, and the optimal variable was determined in wind tunnel testing via the boundary-layer wind profile. The goal of the optimal shape was to reduce the wind pressure at the leading edge of the noise barrier to the level suggested in the Eurocode and to maintain the base-bending moment of the added member at the same level as the noise-barrier section. Using parametric wind tunnel investigation, an added member with a slope of 1:2 that protruded 1.2 times the height of the noise barrier was proposed. This added member is expected to simplify, or at least minimize, the types of column members required to equidistantly support both added members and noise barriers, which should thereby improve the safety and construction convenience of noise-barrier structures.

Keywords: pressure; reduction; noise barrier; wind; free-standing wall

1. Introduction

A free-standing wall is subjected to wind pressure that is larger at the ends than it is in the middle due to suction that is generated at the back (Letchford and Robertson 1999, Robertson *et al*., 1998). The magnitude of the wind pressure that increases at the ends of free-standing walls depends on the wind direction, and Letchford and Holmes (1994) used wind tunnel tests to establish that the increased wind pressure at the ends is largest for a wind direction of 45°. Robertson *et al*. (1996) confirmed that result through field measurement and Robertson *et al*. (1997a) also verified it via CFD analysis. Increases in wind pressure at the ends of free-standing walls are affected not only by wind direction but also by their length. Via wind tunnel tests and field measurements, Letchford and Robertson (1999) and Robertson *et al*. (1996, 1997b) confirmed that the wind pressure at the end of a free-standing wall increases as the ratio of the wall's length to its height becomes higher. Robertson *et al*. (1995, 1996) confirmed that the wind pressure at the ends of a free-standing wall increases as the wall thickness t becomes smaller.

Noise barriers are representatives of free-standing walls that are subject to increases in wind pressure at the leading edge. To reflect increases in the wind pressure at the leading edge of a noise barrier, the Eurocode (European Committee for Standardization, 2005), as shown in Fig. 1(a), requires that the wall be divided into four sections along its length. The Eurocode also suggests measures for reducing wind pressure at the leading edge by using a so-called return corner, which is installed perpendicular to the longitudinal direction of a noise barrier, as shown in Fig. 1(b). The return corner prevents the wind pressure from getting bigger by blocking suction due to vortices generated behind the noise barrier (Giannoulis *et al*. 2012). Another study on the return corner confirmed that the length of the return corner should be at least as long as the height of the noise-barrier wall (Letchford and Robertson 1999). A return corner installed at right angles along a road, however, presents spacing difficulties in urban areas where noise barriers are normally used.

Attempts to reduce the wind pressure have included inclining the noise barrier itself or using a T-shape (Geurts and van Bentum 2010). However, those approaches involve the problem of increasing the bending moment at the bottom of a noise barrier. Letchford and Robertson (1999) also examined other shapes by either reducing the height at the end of a noise barrier by half or by introducing a gap between the ends of two adjoining noise barriers. The conclusion was that these two cases further increased net

*Corresponding author, Ph.D. Professor
E-mail: hokyungk@snu.ac.kr
[a]Post-Doctoral Researcher, Ph.D.
E-mail: swhan@kict.re.kr
[b]Researcher, Ph.D.
E-mail: junyongpark@sit.re.kr
[c]Research Director, Ph.D.
E-mail: ahnss@ex.co.kr

http://www.techno-press.com/journals/was&subpage=7 ISSN: 1226-6116 (Print), 1598-6225 (Online)

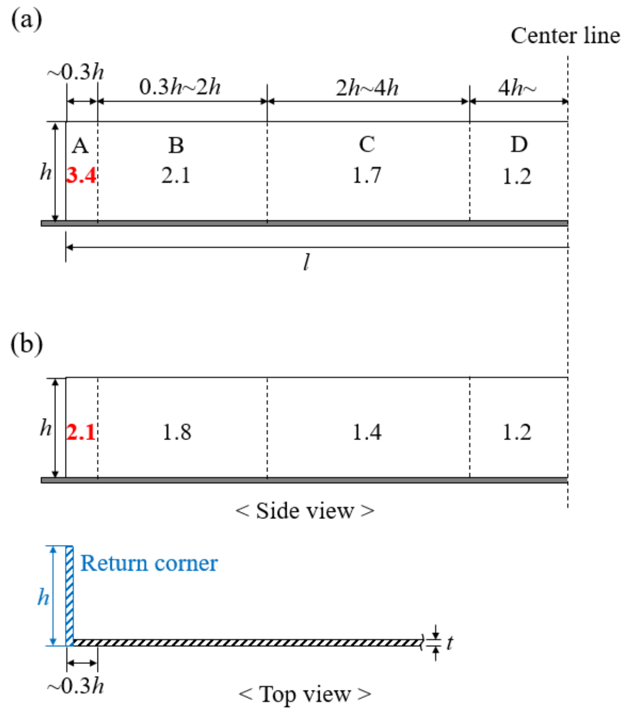

Fig. 1 Pressure coefficients according to the distance from the end of the wall as stipulated by the Eurocode: (a) free-standing walls without a return corner and (b) free-standing walls with a return corner

wind pressure, which is the pressure difference between front and rear sides, at the ends of the noise barriers, and accordingly, more experiments are required to establish that these attempts are helpful. Sato *et al*. (2012) also proposed a new noise barrier equipped with a magnet. When the wind load exceeding the magnet force is applied to the plate, the plate rotates around the top of the noise barrier, and it passes wind and reduces wind load acting on the noise barrier. Another way to reduce wind pressure is to change the solidity of the free-standing wall. Chu *et al*. (2013) and Giannoulis *et al*. (2012) demonstrated the reduction of pressure coefficient according to porosity. In fact, the Eurocode suggests the pressure coefficient of 1.2 regardless of the distance from the leading edge for the free-standing wall with porosity of 20%. However, such porosity can degrade the inherent function of the noise barrier.

In this study, we concentrated on the leading edge of a noise barrier with an added member that would allow a gradual lowering of the height to disperse the wind pressure. When lowering the height of the added member, its shape was defined by finding the optimal variables of length and slope, which were determined in wind tunnel tests using a boundary-layer wind profile. The goal of determining the optimal shape was to reduce the wind pressure at the leading edge of the noise barrier to the level at the return corner and to maintain the base bending moment of the added member at the same level as the noise-barrier section. These developments would simplify, or at least minimize, the types of column members required to equidistantly support both added members and noise barriers. Thereby the safety and construction convenience of noise-barrier structures can be improved, which is important from an engineering point of view.

2. Wind tunnel test setup and data analysis

2.1 Test models and measurement of wind pressure

A model of a prototype noise barrier with a height of 10 m and a length of 80 m was fabricated on a 1/100 scale, which resulted in 10 cm in height and 80 cm in length. The model consisted of eight separate modules 10 cm in height and 10 cm in length. As shown in Fig. 2(a), 25 wind pressure taps were uniformly distributed at intervals of 2 cm on both sides of only one module. Wind pressures were measured by switching the location of this module along the noise barrier. In order to simulate several types of end-treatments by varying the height of a barrier, modules with different heights were also fabricated in units 2 cm in length, as shown in Fig. 2(b). The wind pressure taps were also evenly distributed on those modules. The modules were fabricated with a thickness of 7 mm to accommodate wind pressure tubes inside. The fabricated modules were assembled on a circular disk using connecting bolts, as shown in Fig. 2(d).

The wind tunnel tests were carried out in an Eifel-type wind tunnel operated by the Department of Civil and Environmental Engineering at Seoul National University. The test section of this wind tunnel is 1.5 m in height, 1.0 m in width and 4.0 m in length. The testing model was assembled on a circular disk and installed in the test section, as shown in Fig. 3(a). The circular disk was installed vertically, as shown in Fig. 3(b), which allowed control of the wind direction by rotating the disk. The angle of the wind direction is defined in Fig. 3(a).

The wind pressure taps in the modules were connected to a wind pressure scanner (Model 9IFC, SYSTRA) using a wind pressure tube with a length of 1 m and a diameter of 1.5 mm. It was possible to scan 32 channels simultaneously by the combined use of two 16-channel pressure scanners with frequencies of 500 Hz for two minutes.

2.2 Simulation of the boundary layer

The boundary layer was simulated by assuming the noise barrier would be located in open terrain. A mesh grid, roughness blocks, and air caps were used to simulate a boundary layer, as shown in Fig. 3(a). The mean wind velocity, $\overline{U}$, and the turbulence intensity, defined as the ratio of standard deviation of fluctuating wind velocity to the mean wind velocity, were measured at the position of the leading edge of the noise barrier via a hot-wire anemometer. The profiles along the height were compared with the target values for the case of the wind direction of 45°, as shown in Fig. 4, in which $\overline{U}_{10}$ denoted the mean wind velocity at the height of 10 m. It should be noted that the generated integral length scale at the top of the noise barrier was about 3.3 m based on the prototype scale, which was much smaller than the target value of 100 m

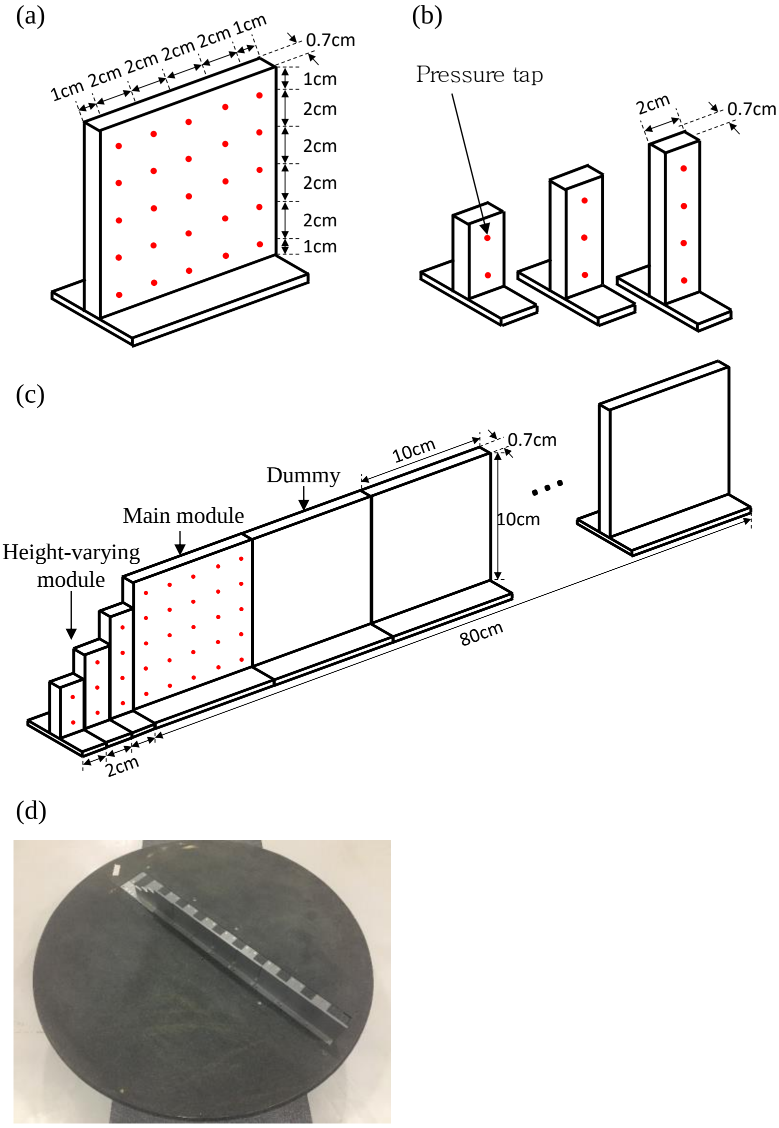

Fig. 2 Wind tunnel test models: (a) main module (b) height-varying module (c) an example of the assembled test model and (d) a turntable for controlling wind directions

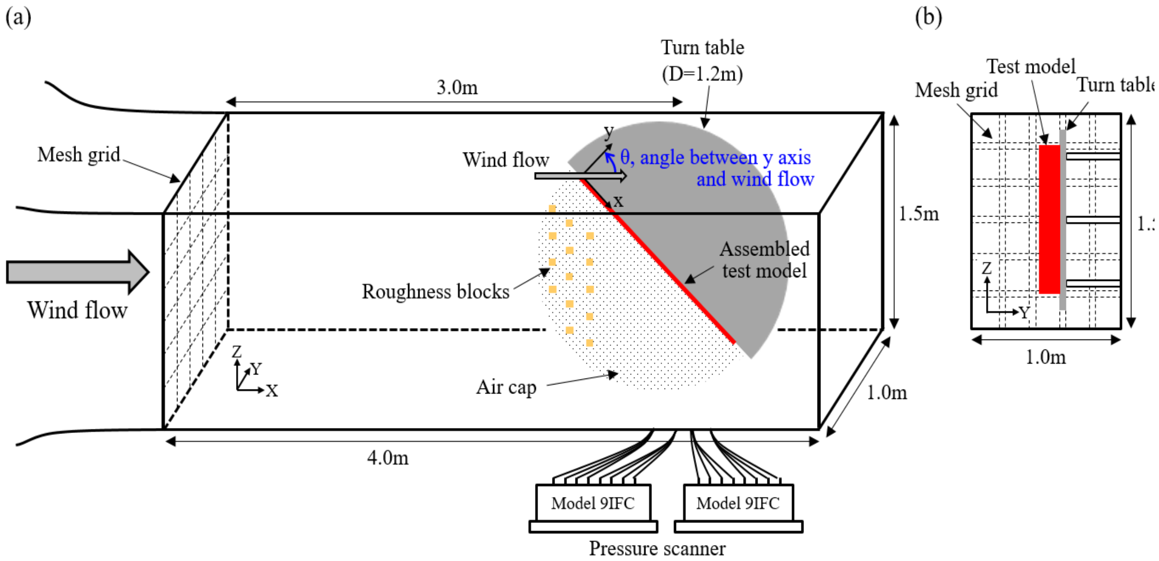

Fig. 3 Wind tunnel test setup: (a) 3D view and (b) 2D (Y-Z plane)

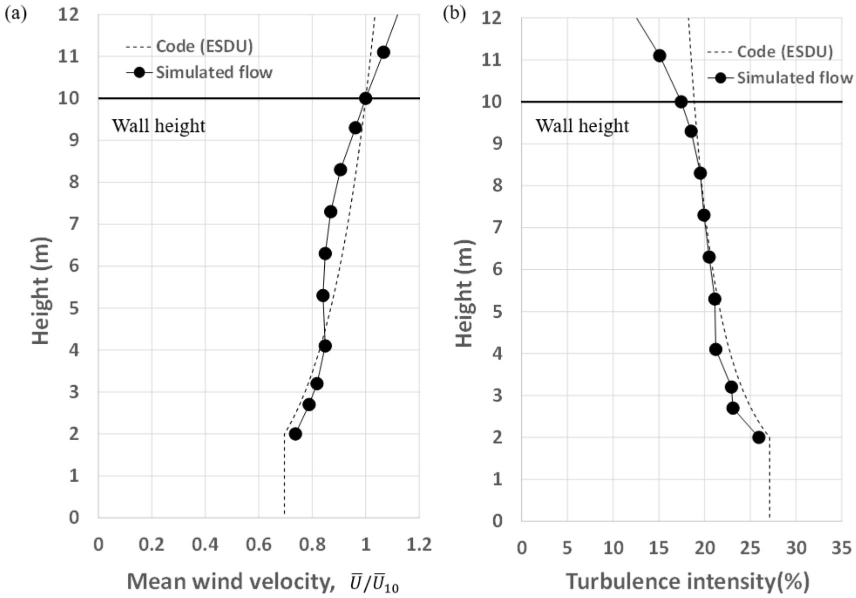

Fig. 4 Simulated boundary-layer profiles in a wind tunnel for: (a) mean wind velocity and (b) turbulence intensity

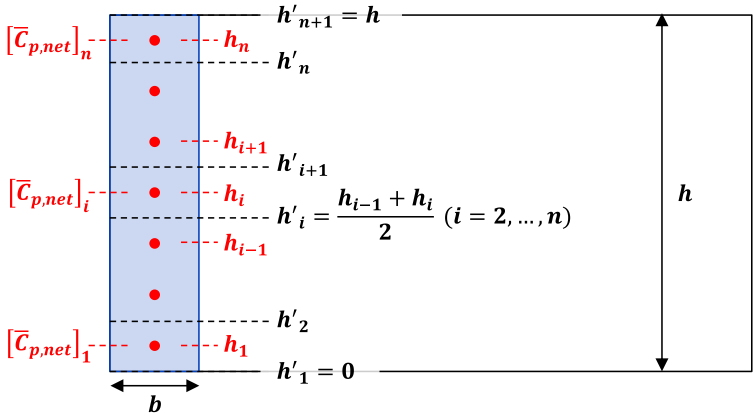

Fig. 5 Definition of variables used in the calculation of $\bar{C}_{p\_a}$ and $\bar{C}_{p\_m}$

(Strømmen 2010). This resulted from the inherent limitations of a small wind tunnel in generating boundary-layer winds, even though the turbulence intensity was successfully realized.

2.3 Definition of resultant pressure coefficients

The effect of the net wind load on the noise barrier could be obtained from the pressure difference between the front and rear pressure taps at a specific point. The front pressure was measured first, and the rear pressure was measured again by flipping over the face of the noise barrier model. The reference pressure was measured under no wind condition. The non-dimensional net pressure coefficient at the i-th tap, $[\bar{C}_{p,net}]_i$, is defined as follows

$$[\bar{C}_{p,net}]_i = \frac{[\bar{p}_{front}]_i - [\bar{p}_{rear}]_i}{\frac{1}{2}\rho \bar{U}_{ref}^2} \tag{1}$$

where i is the position of the pressure taps, which are sequentially increased from the bottom (i=1) of the noise barrier in a specific zone, as shown in Fig. 5. $[\bar{p}_{front}]_i$ and $[\bar{p}_{rear}]_i$ are the measured mean wind pressures at the i-th pressure tap at the front and rear sides of the noise barrier, respectively. ρ is the air density ($= 1.250\text{kg/m}^3$) and $\bar{U}_{ref}$ is the measured mean wind velocity at the reference height, which is regarded as the top of the noise barrier.

Since the wind pressure of the noise barrier varies with height, the introduction of a representative pressure coefficient was useful in demonstrating the overall wind load effect for a specific zone. Two pressure coefficients were defined to represent the resultant wind load effect on the noise barriers. The first pressure coefficient is the area-averaged pressure coefficient ($\bar{C}_{p\_a}$), which denotes an average of the point-pressure coefficients for a specific zone and can be expressed as follows

$$\bar{C}_{p\_a} = \sum_{i=1}^{n} \left[(\bar{C}_{p,net})_i \cdot (h'_{i+1} - h'_i) \cdot b \right] \Big/ (b \cdot h) \tag{2}$$

where b is the width of a specific zone, and h_i is the height of the i-th pressure tap, as shown in Fig. 5. h is the height of

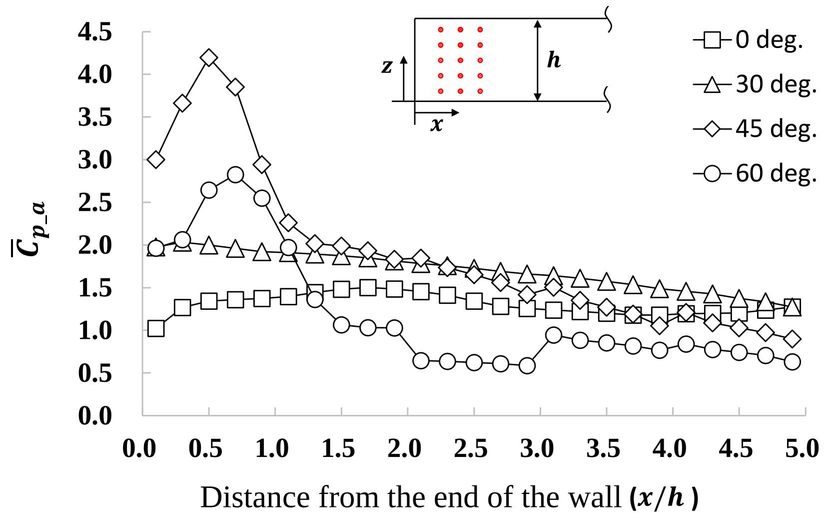

Fig. 6 $\bar{C}_{p\_a}$ along the noise barrier without end-treatment according to various wind directions

the noise barrier and n is the number of pressure taps along the height.

The second pressure coefficient is the moment-averaged pressure coefficient ($\bar{C}_{p\_m}$), which reflects the effect of the equivalent bending moment at the bottom of the noise barrier as follows

$$\bar{C}_{p\_m} = \sum_{i=1}^{n} \left[\left(\bar{C}_{p,net} \right)_i \cdot (h'_{i+1} - h'_i) \cdot h_i \cdot b \right] \Big/ \left(bh \cdot \frac{h}{2} \right) \quad (3)$$

3. Pressure distribution for the noise barrier without end treatment

Prior to the parametric study of the proposed end-treatment shapes, wind tunnel tests were performed to establish a noise barrier without end-treatment in order to obtain data on which to base further comparative study as well to verify the wind tunnel setup and data analysis by comparison with the results of previous studies (Geurts and van Bentum, 2010, Letchford and Holmes 1994, Robertson *et al.* 1997a). Since the wind pressure distribution over the barrier was sensitive to wind direction, four different wind directions were considered: 0, 30, 45, and 60°.

3.1 Distribution of wind pressure

Fig. 6 shows the variations in the area-averaged pressure coefficients, $\bar{C}_{p\_a}$, along the noise barrier for each wind direction. The $\bar{C}_{p\_a}$ near the windward end increased as the wind direction increased. $\bar{C}_{p\_a}$ reached the maximum value at the $x/h = 0.5$ location, particularly for the skewed wind directions of 45 and 60° and quickly decreased toward the center of the noise barrier. On the other hand, relatively uniform wind distributions were identified for the wind directions of 0 and 30°. Since the largest wind pressures at the leading edge of the noise barrier were identified at the wind direction of 45°, which was consistent with previous studies (Letchford and Holmes 1994, Geurts and van Bentum 2010), we used only a wind direction of 45° for further investigation of effective treatment to the windward end of the noise barrier.

Fig. 7 shows the measured distribution of wind pressure on the noise barrier. Figs. 7(b) and (c) show the pressure coefficients of the rear and front sides, respectively, and Fig. 7(a) shows the calculated net pressure coefficient, $\bar{C}_{p,net}$. The overall distribution of $\bar{C}_{p,net}$ near the windward end was similar to the distribution of the pressure coefficient for the rear side of the noise barrier. On the contrary, the distribution of the pressure coefficient on the front side was relatively uniform along the noise barrier. This illustrates how high wind pressure near the end of the noise barrier originates from the suction induced behind the noise barrier. The maximum $\bar{C}_{p,net}$ was identified at the points of $x/h = 0.5$ and $z/h = 0.7$.

Fig. 8 shows the $\bar{C}_{p,net}$ distribution along the height near the windward end and center locations. The values for $\bar{C}_{p,net}$ at the windward ends ($x/h = 0.1, 0.3, 0.5$) were obviously higher than those at the center, as shown in Fig. 8. The $\bar{C}_{p,net}$ near the windward ends showed a higher variation along the height than that near the center. However, the largest amounts of wind pressure were measured at the $z/h = 0.7$ height, regardless of the location along the noise barrier. This is consistent with previous research showing that the wind pressure was greatest at 75% of the wall height (Robertson *et al.* 1995, 1996).

Fig. 9 shows the distribution of $\bar{C}_{p,net}$ along the longitudinal direction of the noise barrier. Regardless of the height of the pressure tap, the maximum $\bar{C}_{p,net}$ occurred at $x/h = 0.5$ measured from the windward end. The wind pressure measured near the bottom of the noise barrier showed a sharp decrease after $x/h = 0.5$, and showed the largest difference in $\bar{C}_{p,net}$ along the height at $x/h = 1.3$. sThe $\bar{C}_{p,net}$ converged to 1.2~1.3 toward the center of the noise barrier regardless of the measurement height. Fig. 9 also shows the resultant pressure coefficients, $\bar{C}_{p\_a}$ and

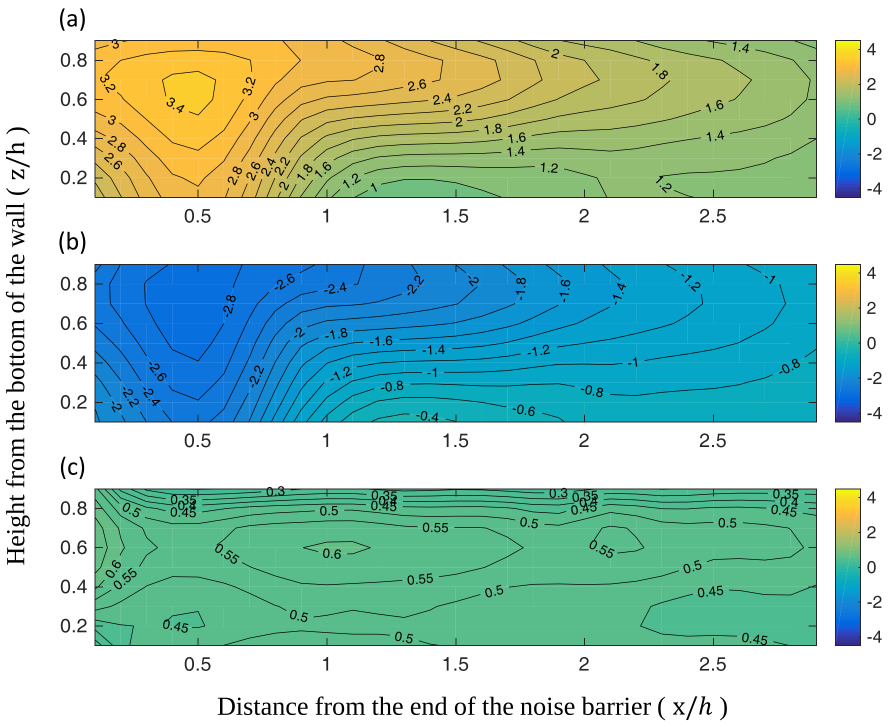

Fig. 7 Distribution of pressure coefficients: (a) $\bar{C}_{p,net}$=$\bar{C}_{p,front} - \bar{C}_{p,rear}$, (b) $\bar{C}_{p,rear}$, wind pressure on the rear side of the noise barrier, and (c) $\bar{C}_{p,front}$, wind pressure on the front side of the noise barrier (wind direction: 45°)

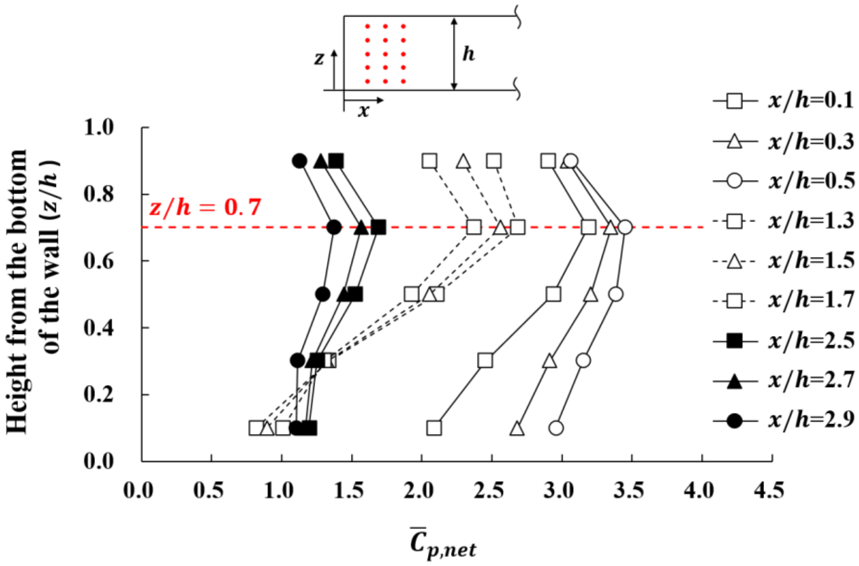

Fig. 8 $\bar{C}_{p,net}$ along the height near the windward end and the center of the noise barrier without end-treatment (wind direction: 45°)

$\bar{C}_{p\_m}$, per unit length of the noise barrier, which are estimated using five different values for $\bar{C}_{p,net}$ along the height. $\bar{C}_{p_m}$was always larger than $\bar{C}_{p\_a}$ due to a relatively larger amount of wind pressure at upper positions of the noise barrier. However, there was little difference between $\bar{C}_{p\_a}$ and $\bar{C}_{p\_m}$ at $x/h = 0.5$, where the net pressure coefficient reached the maximum value. The difference between $\bar{C}_{p\_a}$ and $\bar{C}_{p\_m}$ increased after $x/h = 0.5$. according to the longitudinal distribution characteristics of $\bar{C}_{p,net}$. The distributions of $\bar{C}_{p\_a}$ and $\bar{C}_{p\_m}$ were similar to that of $\bar{C}_{p,net}$ measured at the middle height of the noise barrier.

3.2 Comparison of pressure coefficients

Fig. 10 compares the $\bar{C}_{p\_a}$ distribution in this study

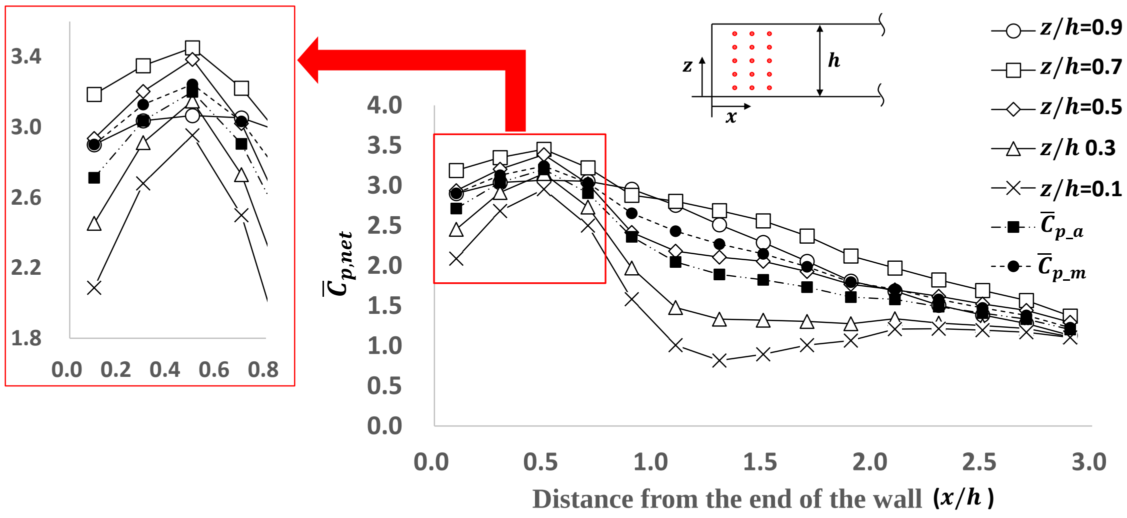

Fig. 9 $\bar{C}_{p,net}$ along the noise barrier at different heights without end-treatment (wind direction: 45°)

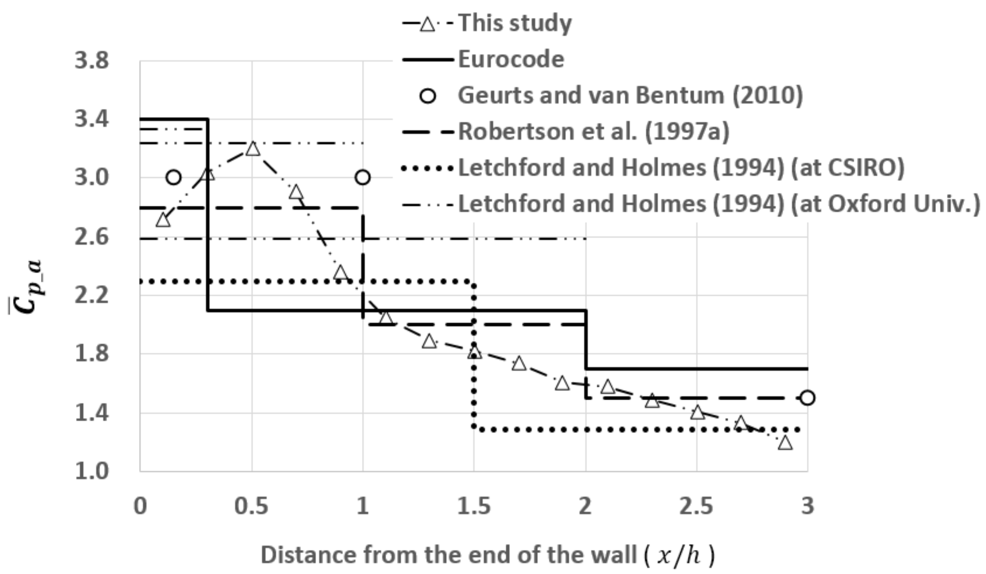

Fig. 10 Comparison of measured $\bar{C}_{p\_a}$

with the mean pressure coefficients of the Eurocode and previous research. The experimental conditions are summarized in table 1. Geurts and van Bentum (2010) estimated the $\bar{C}_{p\_a}$ for specific locations representing zones defined in the Eurocode, as shown in Fig. 1, rather than obtaining a continuous distribution. Robertson *et al.* (1997a) conducted a field test at relatively low turbulence intensity. Letchford and Holmes (1994) conducted wind tunnel tests at both the CSIRO and Oxford University for a noise barrier 5 m in height. The CSIRO wind tunnel test evaluated the $\bar{C}_{p\_a}$ by connecting only six wind pressure taps to one wind pressure tube. The wind tunnel tests at Oxford University evaluated three representative values for $\bar{C}_{p\_a}$ to establish an average concept for categorized zones such as $x/h = 0\sim0.3$, $x/h = 0\sim1.0$ and $x/h = 0\sim2.0$, as shown in Fig. 10. As the pressure coefficients varied dramatically along the noise barrier near the windward end of the noise barrier, the $\bar{C}_{p\_a}$ evaluated from the wind tunnel tests at Oxford University decreased as the averaging area became wider.

In the present study, we installed as many pressure taps as possible along both the length and height of the testing modules to increase the accuracy of the measured pressure distribution. The pressure coefficients in this study generally conformed to those established by Robertson *et al.* (1997a). The pressure coefficients in Fig. 10 show some fluctuations quantitatively, although the overall tendency demonstrates the increased pressure coefficients near the windward end of the noise barrier. The differences may have been induced for several reasons: 1) different locations for pressure taps; 2) different averaging areas for $\bar{C}_{p\_a}$; and, 3) different turbulence intensity in the simulated boundary-layer wind. Shu and Li (2017) found that the magnitude of the suction generated near the windward end of a thin plate decreased as the turbulence intensity increased. Akon and Kopp (2016), for pressures on roofs, also found that the

Table 1 Setup parameters for wind tunnel tests

	Size(m) of wind tunnel (Width x Height x Length)	Size(m) of noise barrier (Height x Length)	Scale of model	Simulation of boundary layer	TI* at the top of noise barrier
This study	1.0 x 1.5 x 4.0	10.0 x 80.0	1 / 100	1) Mesh grid 2) Roughness blocks 3) Air caps	17.5 %
Geurts and van Bentum (2010)	3.0 x 2.0 x 14.0	8.0 x 100.0	1 / 100	1) Upstream fetch 2) Lego board	15.0 %
Robertson et al. (1997a)	Field test	2.0 x 10.0	Prototype	-	13.7 %
Letchford and Holmes (1994) (at CSIRO)	2.0 x 1.0 x 10.0	5.0 x infinite	1 / 75	1) Barrier of 250mm height 2) Surface roughness by carpets	21.0 %
Letchford and Holmes (1994) (at Oxford Univ.)	4.0 x 2.0 x 12.0	5.0 x infinite	1 / 75	1) Coarse wooden grid 2) Surface roughness by inverted plastic cups	24.0 %

*TI: Turbulence Intensity

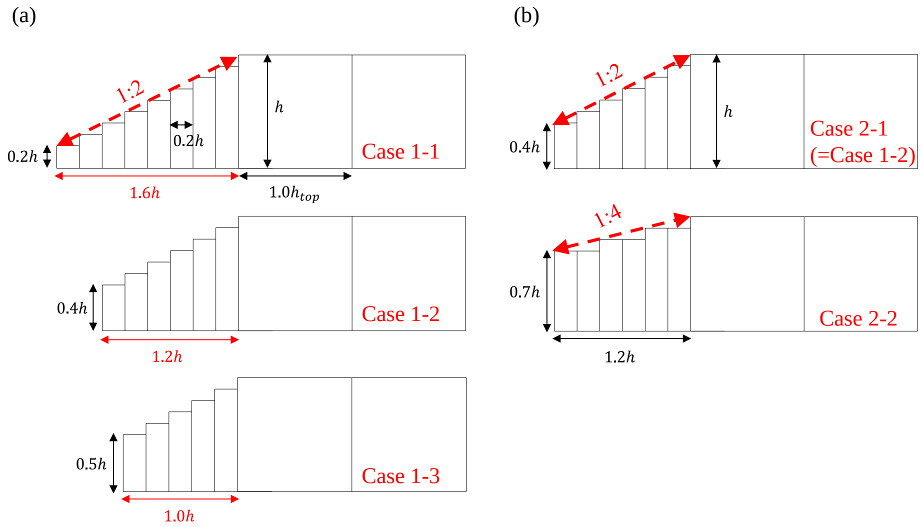

Fig. 11 Variations in the shape of added members examined: (a) Group 1: varying length with a fixed slope and (b) Group 2: varying slope with a fixed length

mean size of the generated suction was unaffected by the turbulence length scales, whereas turbulence intensity had a great influence.

4. Parameter study for an acceptable end treatment of the noise barrier by adjusting the height

In this study we suggested a method to reduce the wind pressure at the windward end of the noise barrier by arranging an added wall that could gradually decrease in height at the tip of the noise barrier. In particular, the effect of the wind load acting on the added wall has been examined by adjusting the height of the wall to within the ultimate acceptable range.

4.1 Examining the shape of an added member

The shape of added members installed at the tip of the noise barrier can be expressed in terms of the length and slope of the height-reduction area. In order to investigate the effect of wind pressure reduction by end treatment using added members, wind tunnel tests were performed on two groups, as shown in Fig. 11.

For the added members of group 1, three cases of varying lengths were considered with the slope fixed at 1:2. As shown in Fig. 11(a), the length of the member added for case 1-1 was 1.6h, and cases 1-2 and 1-3 were set to 1.2h and 1.0h, respectively. In group 2, the slope of the added members was an independent variable, as shown in Fig. 11(b). The length of the added member was fixed at 1.2h, and the slope was changed from 1:2 (cases 2-1 and 1-2) to 1:4 (case 2-2) for further consideration.

4.2 Reduction of wind pressure in group 1

Fig. 12 shows the $\bar{C}_{p,net}$ distribution for group 1. The maximum $\bar{C}_{p,net}$ for cases 1-1, 1-2, and 1-3 were 3.94, 3.94, and 4.53, respectively. The positions of maximum wind pressure were identical in all three cases: $x/h = -0.5$. The wind pressure coefficients at the top of the added members are not clearly shown in Fig. 12 but they converge to zero.

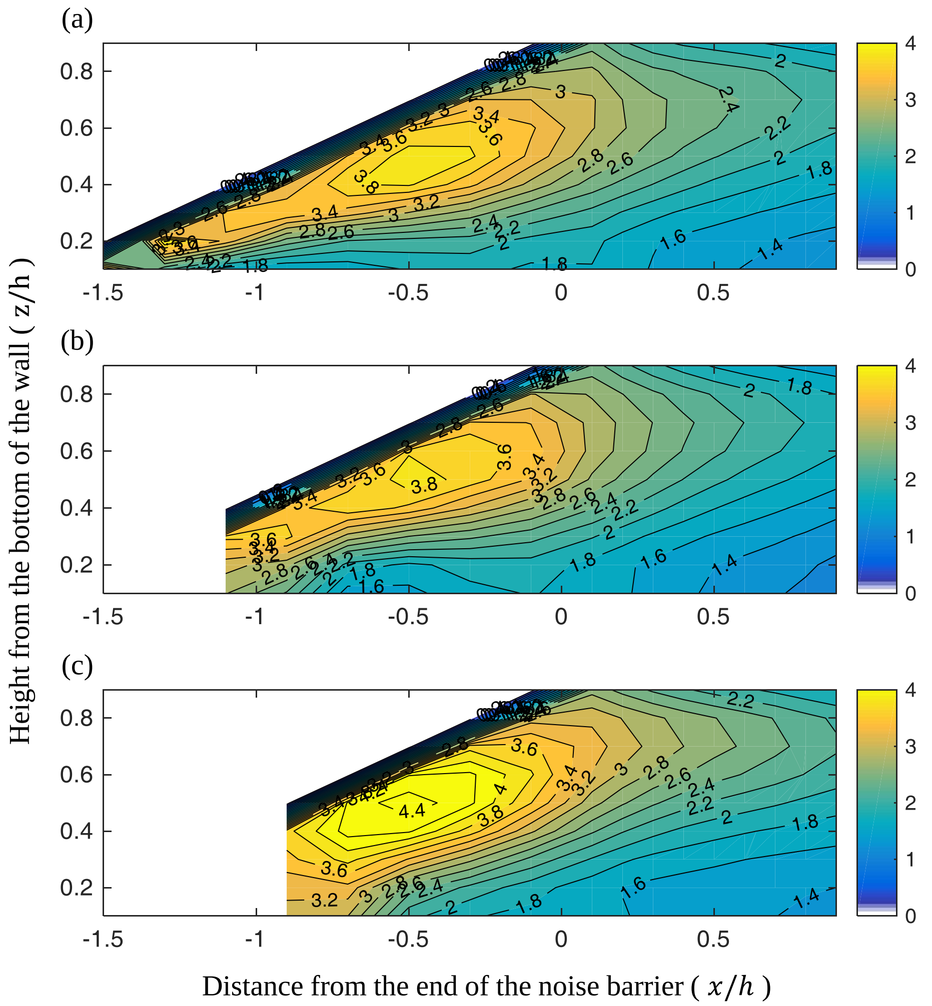

Fig. 12 $\bar{C}_{p,net}$ distribution of group 1: (a) Case 1-1, (b) Case 1-2 and (c) Case 1-3 (wind direction: 45°)

Comparing the wind pressure distributions in cases 1-1 and 1-2 shows that wind pressure is similar in most areas. The wind pressure was rather small for case 1-2, which added a member with a shorter length. These results show that the lower added tip member in case 1-1 did not contribute to a lowering of the wind pressure.

Compared with case 1-2, the length of the added member in case 1-3 was further reduced and the wind pressure coefficient increased. As a result, the wind pressure at the beginning of the noise barrier ($x/h = 0$ to $x/h = 0.3$, Zone A in the Eurocode) was also higher than that of the other cases in group 1.

Case 1-2 set the length of the added member at 1.2 times the height, and was confirmed as the most effective approach in group 1.

4.3 Reduction of wind pressure in group 2

Fig. 13 lists the $\bar{C}_{p,net}$ distribution for group 2, and shows that case 2-1 was identical to case 1-2. Case 2-2, for which the slope was changed to 1:4 while the length was kept at $1.2h$, reduced the maximum wind pressure by about 6.1% from 3.94 to 3.70. However, the maximum wind pressure position shifted somewhat toward the noise barrier at $x/h = -0.5$ to $x/h = -0.3$. Therefore, in case 2-2, the wind pressure was decreased at the lower portion of the noise barrier, but the wind pressure at the upper portion was increased. Increasing the wind pressure at the top increased the bending moment at the bottom of the noise barrier. As a result, cases 2-1 with slopes of 1:2 were more effective.

4.4 Summary of the pressure reduction

The proposed method reduced the bending moment at the lower portion of the added member to an appropriate level and reduced the wind pressure effect on the actual noise barrier. Noise-barrier members are designed by a standardized manner rather than by an individual design, and thus column members are somewhat standardized. Therefore, added members that will be subjected to intense wind pressure are preferably supported by columns of the same size and spacing as those of the noise-barrier section. Table 2 shows the bending moments that were applied to the base of an added member and to the leading edge of the

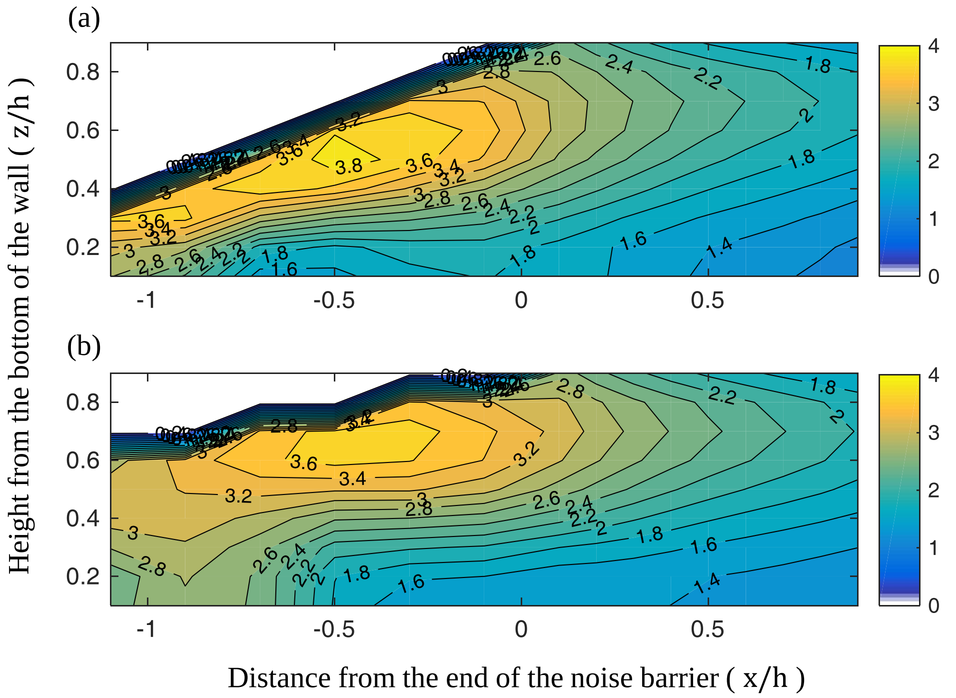

Fig. 13 $\bar{C}_{p,net}$ distribution of group 2: (a) Case 2-1 and (b) Case 2-2 (wind direction: 45°)

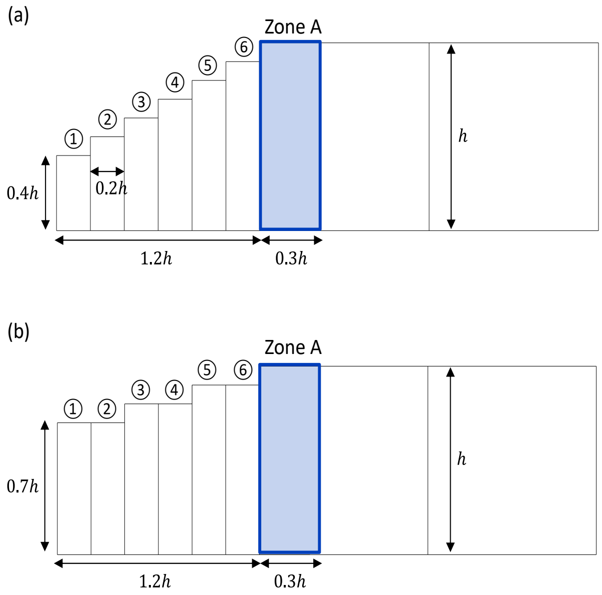

Fig. 14 Numbering (①~⑥) of the end-treatment modules: (a) Case 2-1 and (b) Case 2-2

noise barrier. Refer to Fig. 14 for the location of the members numbered in Table 2. h_{top} is the height of each members numbered in Fig. 14. The wind pressure in case 2-1 was slightly higher than that in case 2-2, but the bending moments at the base of the added member were smaller, and as a result they did not exceed the bending moment at the leading edge of the noise barrier.

Fig. 15 shows the distribution of $\bar{C}_{p\_a}$ for the proposed case 2-1 as well as for the return corner case listed in the Eurocode. Fig. 15 shows that the proposed end-treatment strategy can at least yield wind pressure reduction effects for the return corners, as stipulated in the Eurocode, while also reducing installation space.

5. Conclusions

The effect of reducing the mean wind pressure at the leading edge of a noise barrier was investigated via wind-tunnel testing by varying the length and slope of an added member. Added members with a slope of 1:2 that protruded

Table 2 Moment-averaged pressure coefficients and unit bending moments at the bottom of the noise barriers for group 2

Position (h_{top} of case 2-1 / h_{top} of case 2-2)	① ($0.4h$ / $0.7h$)	② ($0.5h$ / $0.7h$)	③ ($0.6h$ / $0.7h$)	④ ($0.7h$ / $0.7h$)	⑤ ($0.8h$ / $0.7h$)	⑥ ($0.9h$ / $0.7h$)	Zone A
$\bar{C}_{p\_m}$, case 2-1	3.40	3.34	3.15	3.36	3.29	3.05	2.40
Unit bending moment at bottom*, case 2-1	$0.3h^2$	$0.4h^2$	$0.6h^2$	$0.8h^2$	$1.1h^2$	$1.2h^2$	$1.2h^2$
$\bar{C}_{p\_m}$, case 2-2	2.91	3.15	3.24	3.15	3.17	2.99	2.50
Unit bending moment at bottom*, case 2-2	$0.7h^2$	$0.8h^2$	$1.0h^2$	$1.0h^2$	$1.3h^2$	$1.2h^2$	$1.2h^2$

*Unit bending moment at bottom: $\frac{\left[\bar{C}_{p\_m} \cdot bh \cdot \frac{h}{2}\right]}{\mathrm{b}}$

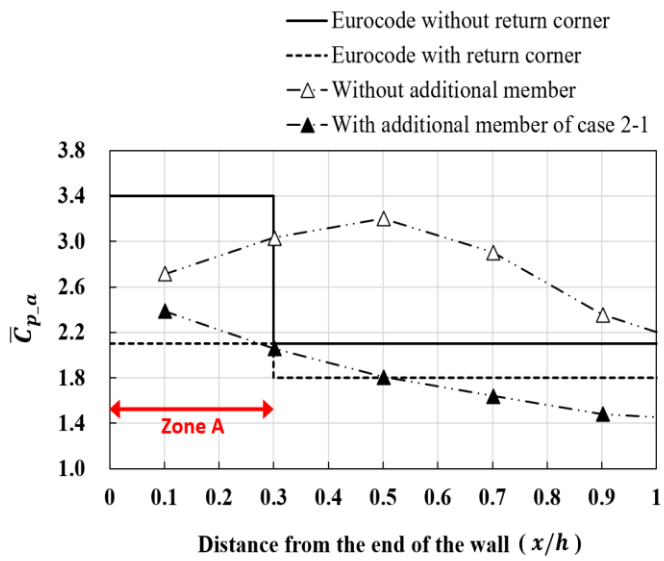

Fig. 15 Comparison of measured $\bar{C}_{p\_a}$ with an added member of case 2-1

1.2 times the height of the noise barrier proved most effective in the review cases. This wind reduction scheme showed that the wind pressure acting on the leading edge of a noise barrier could be reduced to the level of a return corner, as stipulated in the Eurocode. The results of this study also confirmed that the bending moment at the base of the added member should maintain the bending moment level of the noise barrier when the slope of the added member is 1:2. This should simplify, or at least minimize, the types of column members required to equidistantly support the added members and the noise barriers, which should improve the safety and construction convenience of noise-barrier structures. As a follow-up study, the effect of fluctuating components of wind pressure need to be addressed from peak pressure measurement. Field testing is also recommended to verify the effectiveness of the proposed end-treatment via dense application of pressure sensors.

Acknowledgments

This research was supported by grants (Project no. 0583-20150041) funded by the Korea Expressway Corporation Research Institute through the Institute of Construction and Environmental Engineering at Seoul National University.

References

Akon, A.F. and Kopp, G.A. (2016), "Mean pressure distributions and reattachment lengths for roof-separation bubbles on low-rise buildings", *J. Wind Eng. Ind. Aerod.*, **155**, 115-125. https://doi.org/10.1016/j.jweia.2016.05.008.

Chu, C.-R., Chang, C.-Y., Huang, C.-J., Wu, T.-R., Wang, C.-Y. and Liu, M.-Y. (2013), "Windbreak protection for road vehicles against crosswind", *J. Wind Eng. Ind. Aerod.*, **116**, 61-69. https://doi.org/10.1016/j.jweia.2013.02.001.

En, B. (1991), *1-4: 2005 Eurocode 1: Actions on structures-General actions-Wind actions*, NA to BS EN.

Geurts, C. and van Bentum, C. (2010), "Wind loads on T-shaped and inclined free-standing walls", *Wind Struct.*, **13**(1), 83-94. https://doi.org/10.12989/was.2010.13.1.083.

Giannoulis, A., Stathopoulos, T., Briassoulis, D. and Mistriotis, A. (2012), "Wind loading on vertical panels with different permeabilities", *J. Wind Eng. Ind. Aerod.*, **107**, 1-16. https://doi.org/10.1016/j.jweia.2012.02.014.

Letchford, C. and Holmes, J. (1994), "Wind loads on free-standing walls in turbulent boundary layers", *J. Wind Eng. Ind. Aerod*., **51**(1), 1-27. https://doi.org/10.1016/0167-6105(94)90074-4.

Letchford, C. and Robertson, A. (1999), "Mean wind loading at the leading ends of free standing walls", *J. Wind Eng. Ind. Aerod*., **79**(1), 123-134. https://doi.org/10.1016/S0167-6105(97)00292-4.

Robertson, A., Hoxey, R. and Richards, P. (1995), "Design code, full-scale and numerical data for wind loads on free-standing walls", *J. Wind Eng. Ind. Aerod*., **57**(2), 203-214. https://doi.org/10.1016/0167-6105(94)00115-T.

Robertson, A., Hoxey, R., Richards, P. and Ferguson, W. (1997a), "Full-scale measurements and computational predictions of wind loads on free-standing walls", *J. Wind Eng. Ind. Aerod*., **67-68**, 639-646. https://doi.org/10.1016/S0167-6105(96)00106-7.

Robertson, A., Hoxey, R., Short, J., Ferguson, W. and Blackmore, P. (1997b), "Wind loads on boundary walls: Full-scale studies", *J. Wind Eng. Ind. Aerod*., **69-71**, 451-459. https://doi.org/10.1016/S0167-6105(97)00176-1.

Robertson, A., Hoxey, R., Short, J., Ferguson, W. and Blackmore, P. (1998), "Prediction of structural loads from fluctuating wind pressures: Validation from full-scale force and pressure measurements", *J. Wind Eng. Ind. Aerod*., **74-76**(1) 631-640. https://doi.org/10.1016/S0167-6105(98)00057-9.

Robertson, A., Hoxey, R., Short, J., Ferguson, W. and Osmond, S. (1996), "Full-scale testing to determine the wind loads on free-standing walls", *J. Wind Eng. Ind. Aerod*., **60**, 123-137. https://doi.org/10.1016/0167-6105(96)00028-1.

Sato, D., Hansaka, M., Mamada, S. and Taniguchi, N. (2012), "Development of a Wind Load Reduction Soundproof System", *Quart. Report of RTRI*. **53**(3), 180-185. https://doi.org/10.2219/rtriqr.53.180.

Shu, Z. and Li, Q. (2017), "An experimental investigation of surface pressures in separated and reattaching flows: effects of freestream turbulence and leading edge geometry", *J. Wind Eng. Ind. Aerod*., **165**, 58-66. https://doi.org/10.1016/j.jweia.2017.03.004.

Strømmen, E. (2010), *Theory of bridge aerodynamics*, Springer Science & Business Media.

CC